Journal of Materials Chemistry C

PAPER

View Article Online
View Journal | View Issue

Cite this: J. Mater. Chem. C, 2019, 7, 4124

Substantial thermal conductivity reduction in mischmetal skutterudites $Mm_xCo_4Sb_{12}$ prepared under high-pressure conditions, due to uneven distribution of the rare-earth elements†

J. Gainza, [ab] F. Serrano-Sánchez, [a]* J. Prado-Gonjal, [ac] N. M. Nemes, [b] N. Biskup, [bd] O. J. Dura, [e] J. L. Martínez, [a] F. Fauth [f] and J. A. Alonso [a]

Received 21st December 2018,
Accepted 9th March 2019

DOI: 10.1039/c8tc06461j

rsc.li/materials-c

Thermoelectric mischmetal-filled $Mm_xCo_4Sb_{12}$ (Mm: natural cocktail of rare-earth elements, mostly Ce and La) skutterudites have been synthesized and sintered in one step under high-pressure conditions at 3.5 GPa in a piston–cylinder hydrostatic press. Synchrotron X-ray diffraction patterns display a splitting of the diffraction peaks ascribed to purely Ce-, and Mm-filled skutterudite phases, which have been analyzed and confirmed by high-resolution TEM and EELS. A total thermal conductivity (κ) of 1.51 W m^{-1} K^{-1} is measured at 773 K for $Mm_{0.5}Co_4Sb_{12}$, below that of other filled skutterudites, which is promoted by the enhanced phonon scattering over a broad range of the phonon spectrum due to the inhomogeneous and nanoscale mischmetal inclusion. Compared to undoped $CoSb_3$ skutterudite synthesized by conventional methods, κ is reduced by a factor of 3, while the power factor is also substantially enhanced.

Introduction

Thermoelectric materials hold promise for sustainable development by providing a very reliable and clean option for energy conversion from temperature differences. The efficiency of these materials is characterized by the dimensionless figure of merit $ZT = S^2\sigma T/\kappa$, where S is the Seebeck coefficient, σ the electrical conductivity, T the absolute temperature, and κ the total thermal conductivity, which contains the sum of the electronic (κ_e) and the lattice (κ_l) contributions.[1]

Several approaches have been developed to improve thermoelectric efficiency, such as band engineering, nanostructuring, hierarchical architectures, *etc.*[2] Among them, the phonon-glass electron crystal (PGEC) concept proposed by Slack,[3] which describes "rattling" atoms in structural cages, has had a strong impact on thermoelectric research and is one of the main approaches driving the investigation of complex materials like skutterudites. These compounds have attracted much attention recently as a future generation of high-efficiency thermoelectric materials. More precisely, studies based on $CoSb_3$ skutterudites have shown promising features in terms of thermoelectric applications, mainly due to their high electrical mobility and reasonably good Seebeck coefficient.[4] Additionally, tellurium and lead-free materials are of special interest to the thermoelectric community, as the legislations are further restraining the use of these elements.[5,6] Nevertheless, the high thermal conductivity of $CoSb_3$ compounds limits the possible improvements of their general thermoelectric efficiency.

To apply the PGEC approach, different elements have been used to significantly reduce κ_{lat} by filling the empty structural voids at 2a Wyckoff positions of the skutterudite structure,[4] defined in the $Im\bar{3}$ space group (no. 204). Among them, rare-earth elements have been the most successful fillers in terms of optimization of the thermoelectric properties. For instance, Ce has been used in $In_xCe_yCo_4Sb_{12}$ to achieve a κ_l lower than 1.0 W m^{-1} K^{-1} at 800 K.[7] Moreover, single-filled Ce skutterudites displayed very good thermoelectric properties with κ_l around 2.0 W m^{-1} K^{-1} for $Ce_{0.17}Co_4Sb_{12}$ at 850 K, increasing the filling fraction limit using a solubility design.[8]

Nevertheless, since the use of individual rare-earth elements is costly, it is of great importance to find an alternative method with a similar effect. Mischmetal is an alloy of different rare-earth elements that happens in nature in various proportions,

[a] Instituto de Ciencia de Materiales de Madrid (ICMM), Consejo Superior de Investigaciones Científicas (CSIC), Sor Juana Inés de la Cruz 3, E-28049, Madrid, Spain. E-mail: fserrano@icmm.csic.es
[b] Departamento de Física de Materiales, Universidad Complutense de Madrid, E-28040 Madrid, Spain
[c] Departamento de Química Inorgánica, Universidad Complutense de Madrid, E-28040 Madrid, Spain
[d] Instituto Pluridisciplinar, Universidad Complutense de Madrid, E-28040, Spain
[e] Departamento de Física Aplicada, Universidad de Castilla-La Mancha, Ciudad Real, E-13071, Spain
[f] CELLS–ALBA synchrotron, Cerdanyola del Valles, Barcelona, E-08290, Spain

† Electronic supplementary information (ESI) available: XRD patterns, SXRD patterns and structural parameters of nominal $Mm_{0.5}Co_4Sb_{12}$ at high temperature. See DOI: 10.1039/c8tc06461j

mainly formed of R = Ce and La. The resulting multiple-filled skutterudite promotes scattering over a broader range of the phonon spectrum due to the increased disorder and slightly different vibration frequencies, involving further reduction of the lattice thermal conductivity.[9–11] At the same time, it also reduces the final cost of the material, as the individual purification and extraction process of the rare earth is no longer needed.[12] The use of mischmetal as multi-element filler was already studied at low temperature (between 2 and 300 K) by Yang *et al.*,[13] concluding that the figure of merit would improve at higher temperatures. On the other hand, L. Zhang *et al.* characterized Mm-based skutterudites at elevated temperatures, from room temperature up to 800 K, finding no significant changes in the thermal conductivity using Ce ($Ce_yFe_3CoSb_{12}$) or mischmetal ($Mm_yFe_3CoSb_{12}$)[14] as fillers. However, these previous works using mischmetal as a filler report on p-type charge-compensated (Co,Fe)Sb_3-skutterudites; the presence of Fe at Co sites has been demonstrated to considerably alter the thermoelectric properties.[4]

Recently, we studied the structure and thermoelectric transport properties of R_xCoSb_3 (R = La, Ce, or Yb) prepared under high pressure.[15,16] A significant reduction of the thermal conductivity was found as a consequence of the uneven filler distribution in R-poor and R-rich phases at a nanometric scale.[15] This type of reduction was previously attributed to filling fraction fluctuation and consequent strain-field and long-range acoustic phonon scattering by Wei *et al.* in La-filled Fe_4Co_{12} skutterudite.[17]

In this work, we use mischmetal (Mm) as the source of filler elements, instead of pure rare-earth metals. n-Type Mm-filled $CoSb_3$, with no charge-compensation by Fe doping, has not been studied until now: the description of n-type materials, is necessary together with the p-type counterparts for the development of proper thermoelectric devices. We report on the high-pressure synthesis (3.5 GPa) of n-type Mm-filled $CoSb_3$ skutterudites in order to further reduce the lattice thermal conductivity, which is one of the main ingredients of good thermoelectric materials. A synchrotron X-ray diffraction (SXRD) study reveals the phase segregation in Mm- and only-Ce-filled $CoSb_3$ phases within the sample, which has been analyzed and confirmed by high-resolution TEM. This segregation of different filler elements contributes to further reduce the lattice thermal conductivity, from those measured for nominal $La_{0.5}Co_4Sb_{12}$, $Yb_{0.5}Co_4Sb_{12}$ and $Ce_{0.5}Co_4Sb_{12}$ prepared under high-pressure.[15,16] This could be a good starting point to enhance even more the thermoelectric properties in filled skutterudites.

Experimental procedures

Samples with nominal composition $Mm_xCo_4Sb_{12}$ (x = 0.15, 0.20, 0.25, 0.50) were prepared by a solid-state reaction under moderate temperature and high pressure conditions. About 1.2 g of a stoichiometric mixture of the starting elements Mm (min 99.0% of rare-earth content, Alfa Aesar, with a proportion of 75% Ce and 25% La), Co (99%, ROC/RIC) and Sb (99.5%, Alfa Aesar) were carefully ground and placed in a niobium capsule (5 mm diameter), sealed and introduced inside a cylindrical graphite heater. To prevent oxidation, the capsule was properly manipulated inside an Argon-filled glove-box. Reactions were carried out in a piston–cylinder press (Rockland Research Co.), at a pressure of 3.5 GPa, at 800 °C for 1 h. Afterwards, the products were quenched to room temperature and the pressure was released. The samples were obtained as hard pellets, which were partially ground to powder for structural characterization, or cut with a diamond saw as bar-shaped pellets to perform transport measurements. The density of the samples measured by the Archimedes method is found to be ~90% of the theoretical crystallographic density, *ca.* 6.8 g cm^{-3}.

Phase characterization was carried out using X-Ray diffraction (XRD) on a Bruker-AXS D8 diffractometer (40 kV, 30 mA), run by DIFFRACTPLUS software, in Bragg–Brentano reflection geometry with Cu Kα radiation (λ = 1.5418 Å).

In order to analyze the structural details, we have performed temperature-dependent SXRD experiments of a selected $Mm_{0.5}Co_4Sb_{12}$ composition. The MSPD-diffractometer beamline at ALBA synchrotron (Barcelona, Spain) was employed to collect the patterns, using the high angular resolution mode (MAD set-up) with an incident beam of 28 keV energy (λ = 0.4427 Å).[18] The polycrystalline powder was contained in rotating quartz capillaries of 0.7 mm diameter. SXRD patterns were collected at room temperature (RT), 473, 673, 873 and 1073 K for the temperature dependent analysis. A systematic splitting of the diffraction peaks indicates the segregation into two different skutterudite phases with close unit-cell parameters.

TEM images were taken in a JEOL 3000F microscope operated at 300 kV. EELS images were collected in scanning mode using a Gatan Enfina spectrometer. The Scanning Electron Microscope (SEM) images were obtained on a Hitachi instrument, model TM-1000.

The Seebeck coefficient was measured using a commercial MMR-technologies system. Measurements were performed under vacuum (10^{-3} mbar) in the temperature range of 300–700 K. A constantan wire was used as a reference for comparison with bar-shaped skutterudite samples cut with a diamond saw perpendicular to the pressing direction. The reproducibility was checked with different contacts and constantan wires.

A Linseis LFA 1000 instrument was used to measure the thermal diffusivity (α) of the samples over a temperature range of 300 K $\leq T \leq$ 800 K by the laser-flash technique. A thin graphite coating was applied to the surface of the pellet to maximize heat absorption and emissivity. The thermal conductivity (κ) is determined using $\kappa = \alpha \cdot C_p \cdot d$, where C_p is the specific heat and d is the sample density. Specific heat was calculated using the Dulong–Petit equation.

Results and discussion

Structural characterization

Small compact pellets of $Mm_xCo_4Sb_{12}$ were directly obtained from the high-pressure reaction, easily removed from the Nb capsule. Preliminary characterization was performed by XRD of some pellets ground to powder (Laboratory XRD patterns in Fig. 1a).

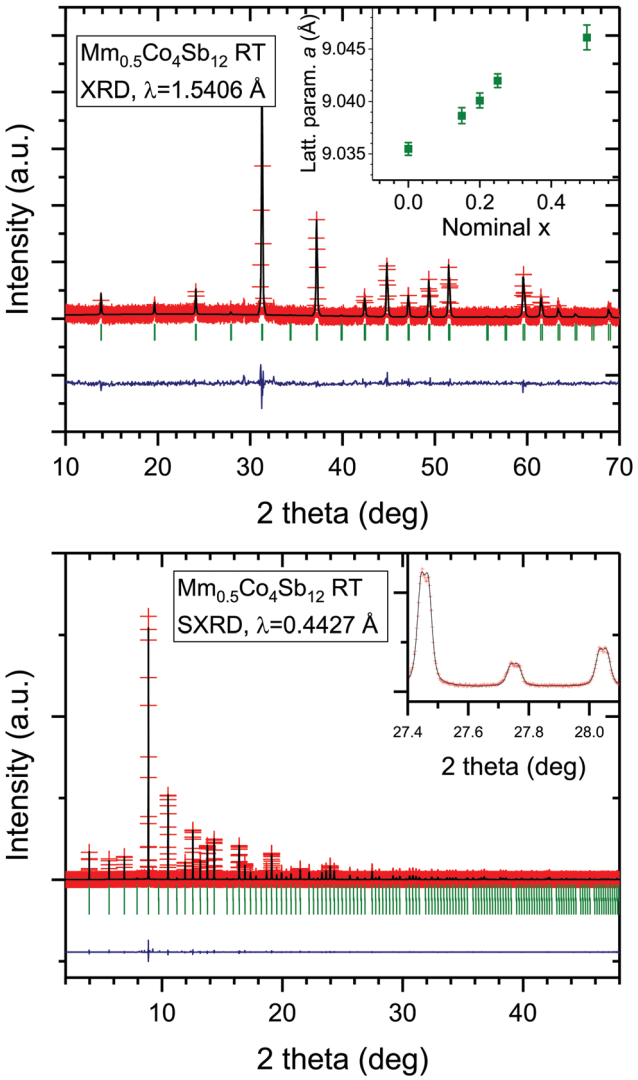

Fig. 1 Experimental points (red crosses), calculated profile (black line), difference (blue line) and Bragg reflections (green symbols), (a) laboratory XRD pattern with Cu K_α radiation. The inset shows the variation of the *a* unit-cell parameter with the nominal *x* content, and (b) SXRD pattern for $Mm_{0.5}Co_4Sb_{12}$ at RT.

The patterns correspond to the skutterudite structure, defined in the space group $Im\bar{3}$; minor $CeSb_2$ impurities were detected from laboratory XRD data. The variation of the lattice parameters of $Mm_xCo_4Sb_{12}$ (x = 0.15, 0.20, 0.25, 0.5) are included in the inset of Fig. 1a. The Rietveld plots from XRD data are shown in Fig. S1 (ESI†).

The high angular resolution of SXRD data was essential to study thoroughly the structural features of $Mm_{0.5}Co_4Sb_{12}$ nominal composition. The crystal structure was refined in the skutterudite $Im\bar{3}$ (#204 space group) model, where Sb atoms are located at 24g (0, y, z), Co at 8c ($\frac{1}{4}$, $\frac{1}{4}$, $\frac{1}{4}$) and Mm at 2a (0, 0, 0) Wyckoff positions. Temperature dependent structural parameters, as lattice parameters, agreement factors and anisotropic displacement parameters, are included in Table 1 and Table S1 (ESI†). Phase fraction and occupancy factors were fixed to the room temperature values. Fig. S2 (ESI†) displays the SXRD patterns at

Table 1 Structural parameters of $Mm_{0.5}Co_4Sb_{12}$ prepared under high-pressure at RT obtained from SXRD data

Nominal composition	$Mm_{0.5}Co_4Sb_{12}$	
Refined composition	$R_{0.08(1)}Co_4Sb_{11.60(9)}$	$R_{0.05(1)}Co_4Sb_{11.74(8)}$
Phase abundance (%)	50.1(9)	49.9(9)
Lattice parameter (Å)	9.04724(4)	9.03936(4)
Volume (Å^3)	740.544(6)	738.610(6)
U_{11} (Co)/Å^2*	0.0050(4)	
U_{12} (Co)/Å^2**	0.0000(5)	
y (Sb)	0.33559(15)	0.33478(15)
z (Sb)	0.15833(14)	0.15759(14)
Occ. Sb (<1)	0.967(8)	0.978(7)
Occ. R (<1)	0.084(9)	0.050(9)
U_{11} (Sb)/Å^2***	0.0055(4)	
U_{22} (Sb)/Å^2	0.0087(5)	
U_{33} (Sb)/Å^2	0.0064(4)	
U_{23} (Sb)/Å^2	0.0011(3)	
U_{11} (R)/Å^2****	0.037(13)	
d Co–Sb (Å)	2.5305(6)	2.5282(6)
d_1 Sb–Sb (Å)	2.8649(18)	2.8490(18)
d_2 Sb–Sb (Å)	2.9749(19)	2.9870(19)
R_p (%)	6.16	
R_{wp} (%)	7.80	
R_{exp} (%)	5.62	
R_{Bragg} (%)	2.12	1.63
χ^2 (%)	1.93	

R_x = Mm (left), Ce (right); Sb at 24g, (0,y,z); Co at 8c ($\frac{1}{4}$,$\frac{1}{4}$,$\frac{1}{4}$); R at 2a (0,0,0); Anisotropic U. Co: * $U_{11} = U_{22} = U_{33}$; ** $U_{12} = U_{23} = U_{13}$; Sb: *** $U_{12} = U_{13} = 0$; R: **** $U_{11} = U_{22} = U_{33}$

different temperatures. The pattern at room temperature (Fig. 1b) is characterized by the splitting of the skutterudite diffraction peaks (inset of Fig. 1b), which is interpreted as two skutterudite phases with different filling fraction and lattice parameters, a. The refinement of the occupation factors yields the compositions $R_{0.08}Co_4Sb_{11.54}$ and $R_{0.05}Co_4Sb_{11.64}$ (R = Ce and/or La) for skutterudites with unit-cell parameters 9.04726(4) and 9.03938(4) Å (Table 1), hereafter called as R-rich and R-poor phases, respectively.

The global refined R content is always lower than the nominal stoichiometry, with total x = 0.13 for nominal x = 0.5. Similar average filling levels have been described elsewhere for La-filled skutterudites.[19] Furthermore, Ce as a filler element, is not so commonly used in single-filled skutterudites, as a consequence of the small filling fraction limit of $Ce_{0.1}Co_4Sb_{12}$.[8,20] The difference with the nominal Mm content can be accounted for by the presence of tiny amounts of $CeSb_2$, which are commonly observed in other reports on filled skutterudites[8,20,21] and has been included in the refinement, corresponding to a fraction of <2%. Besides, negligible Ce impurities are detected in the SXRD patterns (unobservable in the laboratory XRD patterns). The regular variation of the unit-cell parameters (inset of Fig. 1) demonstrates a progressive filling of the skutterudite cages with the nominal Mm amount (x), even if a part of mischmetal remains unreacted. We can speculate that there is a thermodynamic equilibrium that requires an excess of filler to achieve a certain filling fraction.

Strictly speaking, the distribution of R = Ce and La elements from mischmetal in the different phases cannot be distinguished from SXRD data, due to the similar scattering factors of both elements, contiguous in the Periodic Table. However,

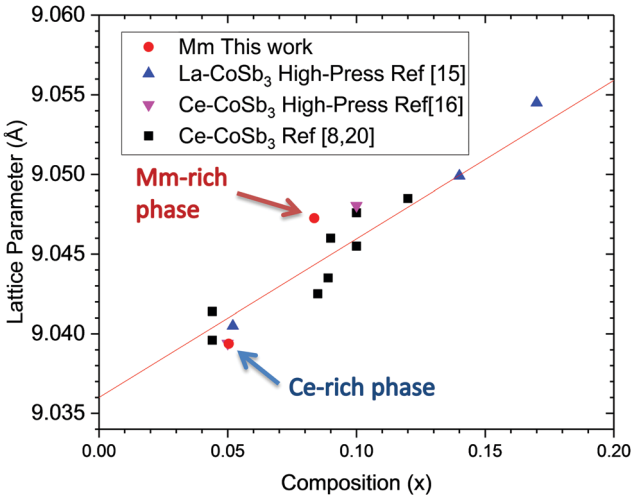

Fig. 2 Lattice parameter dependence with filler fraction and linear fit to previously reported values in ref. 8, 15, 16 and 20.

the lattice parameters of the phases provide us with valuable information about the filling fraction and the size of the cationic filler. It is well known that the variation of the lattice parameter upon filling the skutterudite cages shows a linear dependence on the filling fraction,[8,20] up to a certain filling fraction limit (FFL). This is displayed in Fig. 2, in which the refined parameters of the Mm-filled compound phases are compared to our previous result on La-filled and Ce-filled $CoSb_3$ and literature data. According to this plot, the lattice parameter and filling factor of the R-poor phase exactly matches with a Ce-filled skutterudite phase. On the other hand, a larger increase of the lattice parameter compared to La and Ce-filling suggests a mischmetal-filled (containing both La and Ce atoms) skutterudite, as it has been previously described.[13] We recall that the mischmetal provided by Alfa Aesar contains 75% Ce and 25% La.

Filler atoms have been described to act as "rattlers" caged in a crystalline structure, contributing to a reduced thermal conductivity in skutterudite compounds by resonant scattering of phonons. The picture we obtain from SXRD data is that regions with Ce-only skuttedurite phases are segregated from mischmetal-filled phases; this segregation probably accounts for an additional reduction of the lattice thermal conductivity of this material, if the two phases are mixed on the nanoscale.

In order to avoid correlation effects between occupation factors and atomic displacement parameters, the refinements at high temperature were defined with a fixed occupation (Table S1, ESI†). However, important changes occur above 873 K in the split peaks of the SXRD patterns (Fig. S3, ESI†). The occupation factors and phase ratio have been included in the Rietveld refinement at high temperature, for which the structural data are reported in Table S2 (ESI†). This analysis displays an important variation of the occupancy factors above 873 K. A reduced filling fraction reveals a segregation of the rare-earth elements from the skutterudite structure, and the different phase ratio displays an increase of the R-poor phase abundance. It indicates a thermally activated reorganization of the atomic structure at this temperature and reveals the

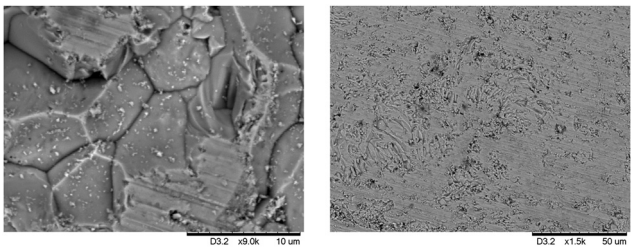

Fig. 3 SEM images of as-grown pellets of $Mm_{0.2}Co_4Sb_{12}$. (a) ×9000 and (b) ×1500 magnification.

metastable nature of these compounds prepared under high pressure. This behavior is only observable above the maximum temperature of the thermoelectric transport measurements. Thus, this effect would not affect thermoelectric performance. As a final test, a sample with composition $Mm_{0.5}Co_4Sb_{12}$ was annealed in vacuum at 873 K during 24 h to analyze the resulting thermal conductivity.

Grain boundary and morphology have been examined by SEM in order to assess the compactness and homogeneity of the samples. Fig. 3 shows different SEM images of a $Mm_{0.2}Co_4Sb_{12}$ sample, with grains on average 10 μm size and a highly compact microstructure, as well-sintered pellets resulting from the high-pressure synthesis. Fig. S4 (ESI†) illustrates more views of the microstructure of this sample.

The nanoscale separation of two phases is illustrated in the electron energy loss spectroscopy (EELS) analysis. Fig. 4 shows the transmission electron microscopy image of a pair of sub-micrometer-size grains and their chemical mapping. The annular

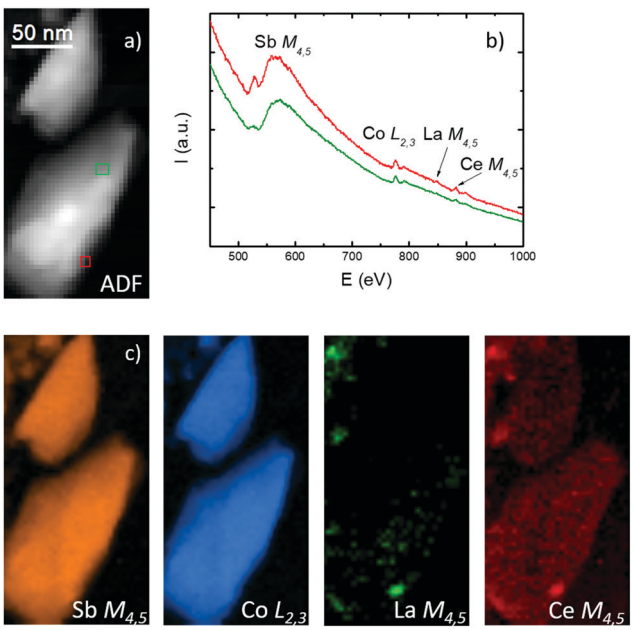

Fig. 4 Elemental mapping of two grains based on EELS analysis. (a) ADF image taken during the EELS acquisition. The red and green rectangles depict the regions from which the two spectra shown in panel (b) are taken. (b) Two spectra with elemental edges indicated. (c) Elemental maps of antimony (yellow), cobalt (blue), lanthanum (green) and cerium (red).

dark field (ADF) image of the grains taken during the EELS acquisition is shown in panel (a). The green and red rectangles in panel (a) show the regions where two representative spectra, shown in panel (b), are taken. EELS edges of all elements are indicated in these spectra. In the spectrum taken from the area of the green rectangle, the Ce $M_{4,5}$ edge can be discerned, but the La $M_{4,5}$ edge is too weak to be detected. On the contrary, in the red rectangle region, both Ce and La edges are stronger, so we are able to detect La signal as well. The elemental maps based on the EELS edges indicated in panel (b) are shown in panel (c). While the Sb, Co and Ce concentration is quite uniform in both grains, the La concentration varies significantly. One can see that, while no La can be detected in the upper grain, the lower grain has nanometer-sized spots with stronger La signal. This indicates that the filling factors of La and Ce are completely different, with La being more prone to concentrate in nanometer-sized spots and in a reduced number of grains. This is very similar to the material analyzed in $La_xCo_4Sb_{12}$ material prepared under similar conditions.[15] On the other hand, the concentration of Ce, in addition to being homogeneous and higher than the concentration of La, is also higher than that obtained in a pure $Ce_xCo_4Sb_{12}$ specimen.[16] This suggests that the Ce filling factor can be increased when La is added to Ce as a doping element for $CoSb_3$. Examination of other six regions (over ten grains) is consistent with these results, as shown in Fig. S5 (ESI†).

Thermoelectric properties

The electrical transport properties of all $Mm_xCo_4Sb_{12}$ samples (prepared under high-pressure conditions) and $CoSb_3$ (prepared by conventional methods) are displayed in Fig. 5. The temperature dependence of the electrical resistivity is shown in the upper panel of this figure. For $x = 0.50$, the resistivity has a maximum around 600 K, and above this temperature it decreases due to the thermal activation of minority carriers across the bandgap. These values could be hampered by the presence of sparse impurities, detected in the SXRD patterns for $x = 0.5$, consequence of the high amount of rare-earth initial content. For $x = 0.15$, the resistivity displays a semiconductor behavior, decreasing monotonously with temperature, from 8.8×10^{-5} Ω m down to 1.5×10^{-5} Ω m. For the two other compositions, $x = 0.20, 0.25$, from RT up to 780 K the resistivity is considerably lower and varies between 8.6×10^{-6} Ω m and 1.1×10^{-5} Ω m, and between 1.09×10^{-5} Ω m and 1.4×10^{-5} Ω m, respectively. These compositions are different: their electrical resistivity increases with temperature, which is the typical behavior of a metallic compound.

These resistivity values are comparable to those reported for Mm-filled and Fe-doped skutterudites, around 1×10^{-5} Ω m,[14,22] yet they are much better (lower) than those measured for undoped HP-synthesized $CoSb_{3-\delta}$, around 2×10^{-4}–3×10^{-4} Ω m,[23] and for $CoSb_3$ prepared by conventional methods, around 2×10^{-4} Ω m. This is due to the charge transfer effect from the filler atoms to the $CoSb_3$ structure.

The Seebeck coefficient (Fig. 5) displays an n-type behavior, with values around −100 μV K^{-1} at room temperature for every composition, as observed for other rare-earth-filled skutterudites.[7,8,16] The absolute Seebeck coefficient slightly increases

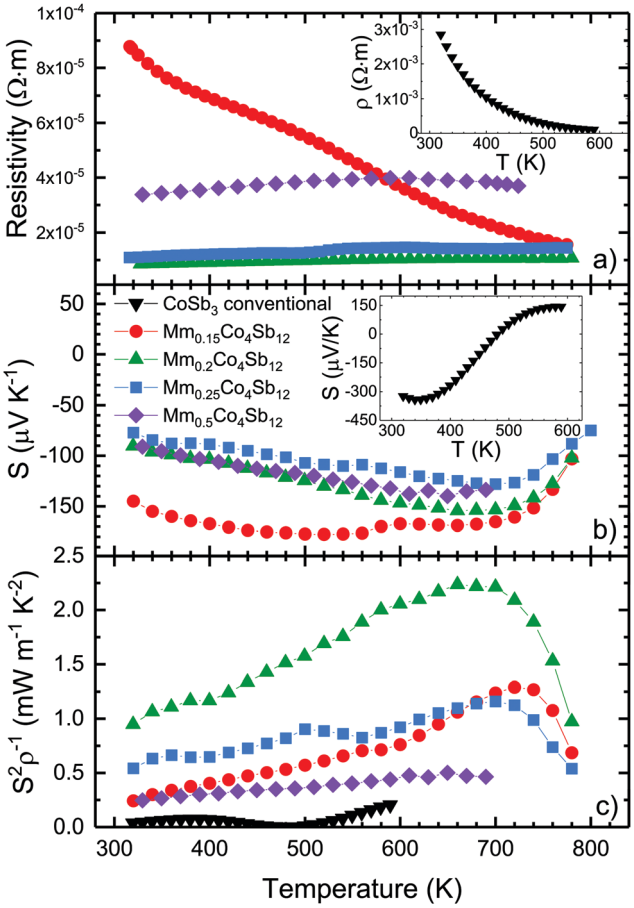

Fig. 5 Temperature dependence of the (a) electrical resistivity, (b) Seebeck coefficient (S) and (c) power factor ($S^2\rho^{-1}$) of $Mm_xCo_4Sb_{12}$ and pure $CoSb_3$ (insets) prepared by conventional methods (from ref. 16).

with temperature, up to a maximum of $S = -155$ μV K^{-1} at 700 K for $Mm_{0.2}Co_4Sb_{12}$. Above that temperature the contribution of minority carriers, cause a decreasing trend. Similar to the electrical resistivity, as a consequence of the charge transfer from the filler atoms to the skutterudite structure, the Seebeck coefficients are reduced compared to $CoSb_{3-\delta}$, obeying the Pisarenko-relation. This is the counterpart of the electrical conductivity enhancement. The trend displayed by the nominal compositions $Mm_xCo_4Sb_{12}$ with $x = 0.15$, 0.20 and 0.25 follows the possible change in the carrier concentration, related to the actual filling level of the skutterudite structure. However, both the resistivity and the Seebeck coefficient of $Mm_{0.5}Co_4Sb_{12}$ could be affected by the presence of impurities.

The power factor (S^2/ρ) was calculated using the experimental values of the Seebeck coefficient and resistivity. As shown in Fig. 5c, a maximum is observed for the $Mm_{0.2}Co_4Sb_{12}$ specimen at relatively high temperatures, reaching 2.25 mW m^{-1} K^{-2} at 660 K. Unlike pure $CoSb_3$, the power factor in Mm-filled $CoSb_3$ indicates a good thermoelectric performance at elevated temperatures, with promisingly elevated power factors.

We obtained important improvements in the skutterudite thermal conductivity (κ_{tot}), as shown in Fig. 6 for $Mm_xCo_4Sb_{12}$ prepared under high-pressure conditions. The best (lowest) κ_{tot}

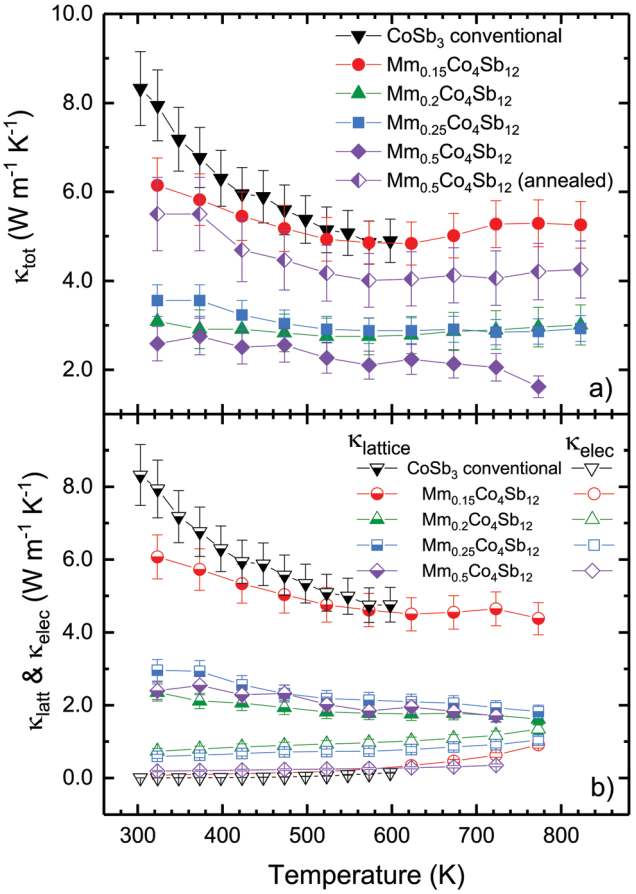

Fig. 6 Temperature dependence of the total thermal conductivity (upper panel), and electronic (κ_e) and lattice (κ_l) contributions (bottom panel) of $Mm_xCo_4Sb_{12}$ and $CoSb_3$ conventional (from ref. 16). Data for an annealed $Mm_{0.5}Co_4Sb_{12}$ sample at 873 K have been included for comparison.

of 1.6 W m^{-1} K^{-1} at 773 K is observed for the $Mm_{0.5}Co_4Sb_{12}$ composition, which is hugely reduced with respect to unfilled $CoSb_3$ skutterudite. However, for $Mm_{0.15}Co_4Sb_{12}$ seems that the actual quantity of mischmetal included in the skutterudite structure is not enough to achieve a great reduction in thermal conductivity, it is still significant compared to the thermal conductivity of the pure $CoSb_3$, of 8.5 W m^{-1} K^{-1} at RT. Moreover, data measured for an annealed $Mm_{0.5}Co_4Sb_{12}$ specimen are included in Fig. 6 for comparison. As commented above for the SXRD at 873 K, at high temperature (*i.e.* during annealing, too) the material becomes homogeneous, since the filler atoms rearrange within the structure, as shown by changes in the phase ratio and filling fractions. The thermal conductivity of the annealed sample is dramatically higher due to the long-range homogenization of the fillers, which endorses the conclusion that it is the phase segregation in the high-pressure synthesized samples that brings about the improved thermoelectric properties. Fig. S6 (ESI†) illustrates the thermal conductivity of $Mm_{0.5}Co_4Sb_{12}$ compound before and after the annealing treatment.

The electronic thermal conductivity was calculated using the Wiedemann–Franz law, which states $\kappa_e = L\sigma T$, being L the Lorentz number, σ the electrical conductivity ($\sigma = \rho^{-1}$) and T the absolute temperature. The value of the Lorentz number was calculated using the expression $L = 1.5 + \exp(-|S|/116)$ (S is in μV K^{-1} and L in 10^{-8} W Ω K^{-2}),[24] giving $L = 1.81 \times 10^{-8}$–2.20×10^{-8} W Ω K^{-2}. As shown in Fig. 6b, the electronic contribution displays a continuous increase with temperature; however, it never reaches a significant value and the phonon contribution dominates the thermal conductivity in most samples, except in $Mm_{0.2}Co_4Sb_{12}$, (and in $Mm_{0.25}Co_4Sb_{12}$) where the electronic and lattice thermal conductivities almost converge at 773 K. This is highly desirable, and occurs because of the low resistivity and lattice thermal conductivity of this compound: the thermal conductivity is no longer dominated by phonons.

The lattice thermal conductivity follows the same temperature trend as the total thermal conductivity. These values (Fig. 6b) are improved (lower) in comparison to that measured for the pure, conventional $CoSb_3$[16] and are also lower than those corresponding to $CoSb_{3-\delta}$, synthesized under high pressure.[23] The comparison with other filled skutterudites and filling fraction indicates that this reduction cannot be exclusively attributed to the filler resonant scattering. In fact, these lattice thermal conductivities are indeed low, even compared to La- and Ce-filled $CoSb_3$ prepared under the high-pressure conditions (~2.5 and 2.8 W m^{-1} K^{-1} at RT, respectively), which display an analogous phase separation, but no elemental segregation.[15,16] As for samples prepared by other means, Nolas *et al.*[25] found lattice thermal conductivity of ~4 W m^{-1} K^{-1} and 7 W m^{-1} K^{-1} in $La_{0.23}Co_4Sb_{12}$ and $La_{0.05}Co_4Sb_{12}$ at 400 K respectively, prepared by a solid state reaction in sealed quartz ampoules. $Ce_xCo_4Sb_{12}$ samples with high actual filling fraction in the range of $x = 0.14$–0.16[8] have values close to 2.0 W m^{-1} K^{-1}, while for samples with $x = 0.05$–0.10 κ_{lat} is *ca.* 4 W m^{-1} K^{-1} at RT.[20] Fu *et al.*[26] measured values between 3.5 (300 K) and 2.0 W m^{-1} K^{-1} (600 K) for Ni-doped $Yb_{0.2}Co_4Sb_{12}$. Other reports of Mm-filled $CoSb_3$ skutterudites include Fe as dopant. These materials are not comparable to our compounds, as the disorder in Co/Fe position induces other effects, additionally reducing the lattice thermal conductivity.[13,14,22] As suggested before, the low lattice thermal conductivity observed in the present high-pressure Mm-filled compounds is not only attributed to the resonant scattering introduced by the filler element, but also to the phase segregation into Ce- and Mm-filled skutterudites. Increased disorder and strain scattering is induced by the uneven distribution of Ce and La atoms in the Mm-filled phase. This low thermal conductivity can be a very interesting starting point to enhance the thermoelectric performance of skutterudite-type materials.

The remarkable increase of the power factor along with the constant reduction of the total thermal conductivity results in an increasing figure of merit up to a maximum of $ZT \sim 0.5$ at 673 K for $Mm_{0.2}Co_4Sb_{12}$ (Fig. 7). Although it can be further improved in mixed Co–Fe skutterudites, the results shown here offer an interesting approach on how a further reduction in thermal conductivity is realized in Co skutterudites upon inducing a segregation of filler atoms of different chemical nature (comparison with the ZT of the annealed sample have been included in Fig. S7, ESI†). In fact, we obtain lattice

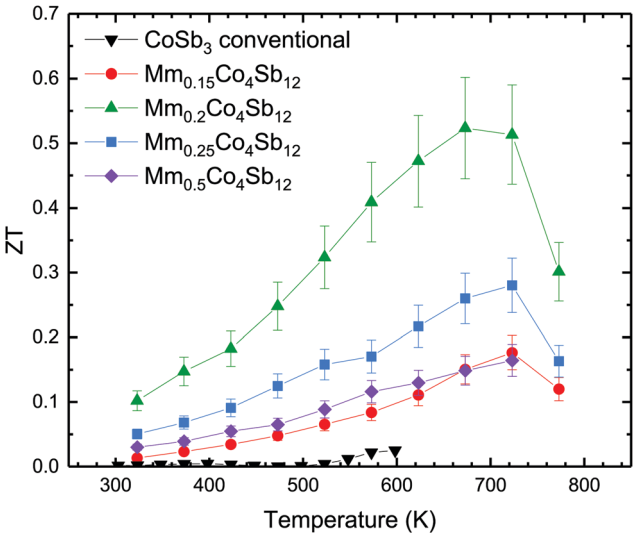

Fig. 7 Temperature dependence of the figure of merit of $MmCo_4Sb_{12}$ and $CoSb_3$. ±15% error bars are included in the graph, based on the accumulation of errors of 5% for the Seebeck coefficient, 5% for the thermal conductivity and 1.5% for the electrical resistivity.

thermal conductivities close to 2 W m^{-1} K^{-1} at RT for our filling fraction, that are as good as these reported for filled skutterudites with a higher filling fraction.[8] Here, this effect spontaneously happens starting from a Ce-rich mischmetal alloy, which under the high-pressure synthesis conditions segregates into Ce-filled and Mm-filled regions. As a final consideration, we have synthesized here Co-only n-type skutterudites; additionally doping with Fe at Co sites, p-type thermoelectric materials can be obtained, where the carrier concentration might be additionally optimized, thus reaching even higher *ZT* figures of merit.

Conclusions

The synthesis and sintering of $Mm_xCo_4Sb_{12}$ skutterudites was carried out in one step under high pressure conditions, followed by quenching. The structural analysis displays an uneven distribution of the different rare-earth elements into Ce-filled and Mm-filled $CoSb_3$ phases. Compared to unfilled $CoSb_3$ prepared by conventional methods, this composition presents an improved resistivity and holds the Seebeck coefficient around ~100–150 μV K^{-1} throughout the whole temperature range, which leads to an enhanced power factor. The inclusion of mischmetal in the structure boosts the scattering over a broader range of phonon spectrum, which results in an exceptional reduction in total thermal conductivity to values as low as 1.6 W m^{-1} K^{-1} at 773 K for $x = 0.5$. This is lower than that found in other Ce- and La-filled $CoSb_3$ skutterudites with even higher filling fractions, which can be attributed to the distribution of the different filler elements into two skutterudite phases, driving the induced disorder and strain field scattering. The best figure of merit, *ZT*, corresponding to $Mm_{0.2}Co_4Sb_{12}$, continuously grows from room temperature up to 673 K, reaching a maximum value of ~0.5, much higher than the original $CoSb_3$ figure of merit. These results show how to further reducing the lattice thermal conductivities of skutterudites while, at the same time, the charge transfer and electronic conductivity properties may be suitably improved to achieve optimized figures of merit.

Conflicts of interest

There are no conflicts to declare.

Acknowledgements

This work was supported by the Spanish Ministry of Science, Innovation and Universities through grants MAT2017-84496-R, MAT2017-87134-C2-2-R and MAT2015-66888-C3-3-R co financed by FEDER. JPG would also like to thank this Ministry for granting a "Juan de la Cierva" fellowship and to Community of Madrid for granting an "Atracción de Talento" fellowship (2017-T2/I ND-5597). Financial support from the ERC grant PoC2015-MAGTOOLS is also acknowledged. The authors wish to express their gratitude to ALBA technical staff for making the facilities available for the synchrotron X-ray diffraction experiment number 2017072260. Transmission electron microscopy studies were performed at the ICTS ELECMI node at Centro Nacional de Microscopía Electrónica (CNME) at the Universidad Complutense de Madrid (UCM).

References

1 G. J. Snyder and E. S. Toberer, *Nat. Mater.*, 2008, **7**, 105–114.
2 J. He and T. M. Tritt, *Science*, 2017, **357**, eaak9997.
3 D. M. Rowe, *Renewable Energy*, 1999, **16**, 1251–1256.
4 M. Rull-Bravo, A. Moure, J. F. Fernández and M. Martín-González, *RSC Adv.*, 2015, **5**, 41653–41667.
5 *DIRECTIVE 2002/95/EC OF THE EUROPEAN PARLIAMENT AND OF THE COUNCIL of 27 January 2003 on the restriction of the use of certain hazardous substances in electrical and electronic equipment*.
6 *COMMISSION DIRECTIVE 2011/37/EU of 30 March 2011 amending Annex II to Directive 2000/53/EC of the European Parliament and of the Council on end of-life vehicles*.
7 H. Li, X. Tang, Q. Zhang and C. Uher, *Appl. Phys. Lett.*, 2009, **94**, 2007–2010.
8 Y. Tang, R. Hanus, S. Chen and G. J. Snyder, *Nat. Commun.*, 2015, **6**, 7584.
9 X. Shi, J. Yang, J. R. Salvador, M. F. Chi, J. Y. Cho, H. Wang, S. Q. Bai, J. H. Yang, W. Q. Zhang and L. D. Chen, *J. Am. Chem. Soc.*, 2012, **134**, 2842.
10 X. Shi, H. Kong, C. P. Li, C. Uher, J. Yang, J. R. Salvador, H. Wang, L. Chen and W. Zhang, *Appl. Phys. Lett.*, 2008, **92**, 1–4.
11 L. Zhang, A. Grytsiv, P. Rogl, E. Bauer and M. Zehetbauer, *J. Phys. D: Appl. Phys.*, 2009, **42**, 225405.
12 F. Habashi, *Can. Metall. Q.*, 2013, **52**, 224–233.

13 J. Yang, G. P. Meisner, C. J. Rawn, H. Wang, B. C. Chakoumakos, J. Martin, G. S. Nolas, B. L. Pedersen and J. K. Stalick, *J. Appl. Phys.*, 2007, **102**, 083702.
14 L. Zhang, A. Grytsiv, M. Kerber, P. Rogl, E. Bauer and M. Zehetbauer, *J. Alloys Compd.*, 2010, **490**, 19–25.
15 F. Serrano-Sánchez, J. Prado-Gonjal, N. M. Nemes, N. Biskup, M. Varela, O. J. Dura, J. L. Martínez, M. T. Fernández-Díaz, F. Fauth and J. A. Alonso, *J. Mater. Chem. A*, 2018, **6**, 118–126.
16 F. Serrano-Sánchez, J. Prado-Gonjal, N. M. Nemes, N. Biskup, O. J. Dura, J. L. Martínez, M. T. Fernández-Díaz, F. Fauth and J. A. Alonso, *ACS Appl. Energy Mater.*, 2018, **1**, 6181–6189.
17 W. Ren, H. Geng, Z. Zhang and L. Zhang, *Phys. Rev. Lett.*, 2017, **118**, 245901.
18 F. Fauth, R. Boer, F. Gil-Ortiz, C. Popescu, O. Vallcorba, I. Peral, D. Fullà, J. Benach and J. Juanhuix, *Eur. Phys. J. Plus*, 2015, **130**, 160.
19 X. Shi, S. Bai, L. Xi, J. Yang, W. Zhang, L. Chen and J. Yang, *J. Mater. Res.*, 2011, **26**, 1745–1754.
20 D. Morelli, G. Meisner, B. Chen, S. Hu and C. Uher, *Phys. Rev. B: Condens. Matter Mater. Phys.*, 1997, **56**, 7376–7383.
21 P. Qiu, X. Shi, Y. Qiu, X. Huang and S. Wan, *Appl. Phys. Lett.*, 2013, **062103**, 2–6.
22 T. Dahal, S. Gahlawat, Q. Jie, K. Dahal, Y. Lan, K. White and Z. Ren, *J. Appl. Phys.*, 2015, **117**, 0–8.
23 J. Prado-Gonjal, F. Serrano-Sánchez, N. M. Nemes, O. J. Dura, J. L. Martínez, M. T. Fernández-Díaz, F. Fauth and J. A. Alonso, *Appl. Phys. Lett.*, 2017, **111**, 1–6.
24 H. S. Kim, Z. M. Gibbs, Y. Tang, H. Wang and G. J. Snyder, *APL Mater.*, 2015, **3**, 041506.
25 G. Nolas, J. Cohn and G. A. Slack, *Phys. Rev. B: Condens. Matter Mater. Phys.*, 1998, **58**, 164–170.
26 L. Fu, J. Yang, J. Peng, Q. Jiang, Y. Xiao, Y. Luo, D. Zhang, Z. Zhou, M. Zhang, Y. Cheng and F. Cheng, *J. Mater. Chem. A*, 2015, **3**, 1010–1016.